

Understanding Disorder in 2D Materials: The Case of Carbon Doping of Silicene

Ricardo Pablo-Pedro, Miguel Angel Magaña-Fuentes, Marcelo Videia, Jing Kong, Mingda Li, Jose L. Mendoza-Cortes,* and Troy Van Voorhis*



Cite This: *Nano Lett.* 2020, 20, 6336–6343



Read Online

ACCESS |



Metrics & More



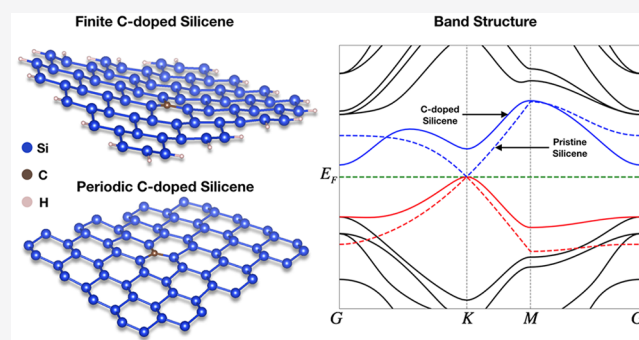
Article Recommendations



Supporting Information

ABSTRACT: We investigate the effect of lattice disorder and local correlation effects in finite and periodic silicene structures caused by carbon doping using first-principles calculations. For both finite and periodic silicene structures, the electronic properties of carbon-doped monolayers are dramatically changed by controlling the doping sites in the structures, which is related to the amount of disorder introduced in the lattice and electron–electron correlation effects. By changing the position of the carbon dopants, we found that a Mott–Anderson transition is achieved. Moreover, the band gap is determined by the level of lattice disorder and electronic correlation effects. Finally, these structures are ferromagnetic even under disorder which has potential applications in Si-based nanoelectronics, such as field-effect transistors (FETs).

KEYWORDS: Disorder effects, chemical doping, formation energies, phase transition



INTRODUCTION

From the large variety of two-dimensional (2D) materials that exist today, silicene, the silicon counterpart of graphene, has steadily increased its sphere of influence due to its malleable electronic properties and its compatibility with the current silicon-based technology.¹ For instance, the buckled layer geometry of silicene facilitates a band gap engineering and in the presence of an electric field opens a gap transport that makes possible the realization of a field-effect transistor (FET) at room temperature.² Synthesis of silicene is achieved nowadays by surface-assisted epitaxial growth on different substrates;^{3–5} however, during this process, the formation of imperfections on the layer is practically unavoidable, which strongly influences the magnetic and electronic properties of the material.^{6–10} In the context of imperfections, these modifications of the electronic, magnetic, and structural properties imply a fundamental form of disorder.¹¹

To illustrate the origin and impact of disorder in silicene, we use chemical doping substitution since it is the simplest way of introducing disorder and of modifying 2D materials' electronic and structural properties beyond electrically controlled means.^{12,13} Unlike graphene, silicene's monolayers are also particularly sensitive to alterations in the geometry of the lattice due to their inherent buckling structure; moreover, silicene's monolayers present two parallel sublattices which induces symmetry breaking between them when defects are introduced. This symmetry between the sublattices produces a

position dependence when more than one defect is introduced. Different arrangements have distinct electronic properties. These geometry and symmetry considerations make silicene prone to a diverse range of phase transitions. Depending on the concentration, distribution, and nature of the doping atoms, the monolayers undergo semimetal to semiconductor or metal transitions.

Consider, for instance, the case of phosphorus-doped silicon (3D structure), a particularly well-studied example of a system showing a metal–insulator transition (MIT).¹⁴ According to Mott's argument, a transition from an insulator to metal occurs at a critical concentration, n_c .¹⁵ Although a temperature, $T = 0$, is necessary for the MIT, several physical systems have shown an MIT at finite temperatures,^{16–18} hence the importance of studying this transition. An MIT which is driven mostly by the electronic correlations is known as a Mott–Hubbard transition,¹⁹ while an Anderson transition is driven mostly by lattice disorder.²⁰

The semimetallic character of silicene limits its potential as a suitable material for distinct applications; however, this

Received: April 23, 2020

Revised: July 28, 2020

Published: July 29, 2020



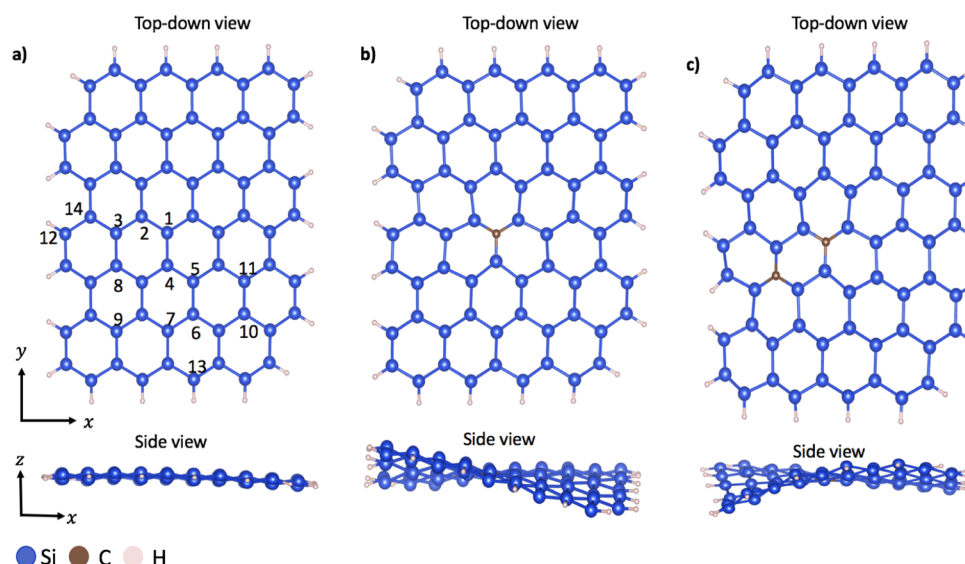


Figure 1. Equilibrium structures of a pure, single-, and double-doped silicene nanocluster. (a) Pure silicene nanocluster, which has 14 nonequivalent possible doping positions. (b) Silicene single-doped with carbon generates out-of-plane distortion. (c) Double-doped carbon substitution generates both out-of-plane and bonds distortions.

limitation could be overcome by the induction of Mott–Hubbard or Anderson transitions. Various authors have studied in detail silicene–graphene hybrid layers and their properties;^{21,22} however, to the best of our knowledge, there is no systematic study on the behavior of carbon-doped silicene in simulations or experiments. In this work, we study the doping behavior of both finite and periodic structures of silicene with carbon atoms. We show that the electronic properties of carbon-doped silicene structures depend on disorder effects and electron–electron correlations. Also, we found that C-doped periodic structures are more stable than monovacancies. Furthermore, we compare the electronic and structural properties of periodic and finite-size structures to have a better understanding of the influence of dopant atoms on the nanoclusters.

AB Initio Characterization. For finite-size structures, we choose the pairing of the Beck 3-Parameter (exchange), Lee, Yang, and Parr (B3LYP) functional with the correlation consistent polarized valence double- ζ (cc-pVDZ) base, along with D3 dispersion correction,²³ as implemented in Q-Chem 5.0.²⁴ For the periodic structures, the numerical simulations were carried out using plane-wave basis as implemented in the Vienna *ab initio* simulation package (VASP).^{25–29} The kinetic energy cutoff for plane waves is set to 500 eV after convergence tests. B3LYP and Perdew–Burke–Ernzerhof (PBE) functionals were used for the periodic structure calculations to compare our results. For the PBE functional, the generalized gradient approximation (GGA) is carried out.

RESULTS AND DISCUSSION

First, we study the geometrical and electronic properties of a rectangular silicene nanocluster with monohydrogen termination at its edges (H-SiNC), see Figure 1a. The selection of these specific structure was based on ref 30 which states that finite rectangular silicene nanoclusters with an armchair edge length (L_a) larger than the zigzag edge length (L_z) could only present ferromagnetic states that when combined with silicon-based semiconductor technology could be valuable for spintronic applications. Different shapes can form different

electronic states, see the Supporting Information for more details. Here, we selected 14 inequivalent doping positions S_1 – S_{14} for a single C atom; then, to study the stability of the doped structures, the defect formation energy, E_f per dopant is calculated using the following equation:

$$E_f = E_d - E_{ud} + nE_{Si} - nE_C \quad (1)$$

where E_d is the total energy of a doped structure, E_{ud} is the energy of a pristine structure, n is the number of dopants, and the E_{Si} and E_C represent the energy of the free Si and C atoms. The formation energies for single carbon substitutions are listed in Table 1. Here, the singlet (antiferromagnetic) and triplet (ferromagnetic) states are reported since C-doped structures can be present in either state. The negative formation energies show that C-doped systems are thermodynamically stable. For a single C substitution, the formation

Table 1. Formation Energies (in eV per impurity atom) of a Single C Substitution at 13 Different Sites of H-SiNC for Singlet (S) and Triplet (T) States at the B3LYP Level of Calculation^a

site	1-carbon (S)	1-carbon(T)
1	−2.266	−2.421
2	−2.331	−2.468
3	−2.456	−2.585
4	−2.271	−2.422
5	−2.294	−2.431
6	−2.327	−2.498
7	−2.526	−2.660
8	−2.468	−2.607
9	−2.600	−2.748
10	−2.532	−2.681
11	−2.474	−2.614
12	−3.372	−3.495
13	−3.233	−3.353
14	−2.849	−2.997

^aAll formation energies were calculated with respect to the singlet undoped ground state of H-SiNC(4,6).

energy increases for sites S_1 , S_4 , S_5 , S_6 , S_2 , S_3 , S_8 , S_{11} , S_7 , S_{10} , S_{14} , S_{13} , and S_{12} , respectively. This shows that Si atoms closer to the edge are more likely to be substituted than those in the interior sites around the zigzag or armchair directions. Similar conclusions were obtained for N- and B-doped silicene nanoribbons.³¹ Figures 1b and 1c illustrate how C substitutions to two silicene structures induce significant distortions caused by disorder; see the Supporting Information for quantification of the disorder in the structures. In addition to the in-plane distortion, a large vertical bending is observed, indicating that the disorder caused by C doping is of long range. In particular, position 1 exhibits the highest buckling distortion, which can extend afar from the substitution site since most of the distortions are elastic. Also, the farther away from the nanocluster's center the more stable the structure becomes and the less disorder it presents. Furthermore, all of the doped configurations prefer to be in a triplet state, indicating that these structures are ferromagnetic and stable under disorder. This intrinsic magnetism is an advantage since it is required for spin-based electronics,^{32,33} particularly for information technology.³⁴

When a carbon atom replaces a silicon one, there is a redistribution of the electronic charge in the system. To illustrate this effect, we show the spatial spin density distribution in Figure 2 for both singlet and triplet states at

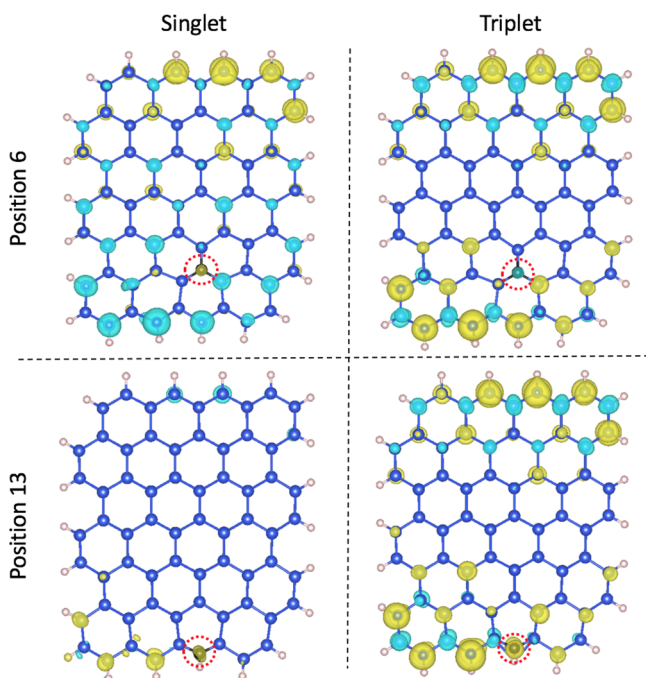


Figure 2. Spin density distributions for a single C-doped H-SiNC at two different site positions. The yellow (cyan) isosurface corresponds to the predominant spin-up (spin-down) charge density. The red circle highlights the position of the carbon atom in the silicene nanocluster.

two different sites. For position S_6 , the singlet state exhibits a negative (positive) magnetic moment at the upper (lower) edge and a zero net magnetic moment, indicating that at this position the C atom does not have a strong effect in the spin density compared with the pristine H-SiNC.³⁵ In the triplet state, the nanoclusters now exhibit a net magnetic moment, having the spins paired-up at opposite edges. For the S_{13}

position in the singlet state, the spin density on the edge is locally concentrated. It is worth noting that such a spin density modification effect is also found in the other inner substitution configurations, but it is gradually weakened as the C atom gets closer to the center of the nanocluster.

For two carbon substitutions, there will be new interactions that can lead to nontrivial effects in the electronic structure. To measure these interaction effects between two carbon atoms, one of them is fixed at position S_{12} (the most stable position) while the other sites are varied. The formation energies for double C-doped structures are listed in Table 2 for singlet and triplet states. All of these structures are thermodynamically favorable, confirming that double C-doped H-SiNCs are stable. We also compare the stability of double versus single C-doping by contrasting the energies $E_f(S_i + S_{12})$ with respect to $E_f(S_{12}) + E_f(S_i)$ with $i = 1, \dots, 14$. With the condition $|E_f(S_i + S_{12}) - [E_f(S_{12}) + E_f(S_i)]| > 1$ eV, only the S_1 , S_2 , S_3 , S_4 , and S_8 positions can be stable for both singlet and triplet state configurations. Similarly to the single C-doping case, the formation energies increase as we move toward the center of the nanocluster. For the adjacent doping cases, $S_{12}-S_{14}$, the C—C bond introduces a higher strain into the structures, due to its shorter length, making those nanoclusters the most unstable ones. Additionally, we have included quintuplet states for the double C-doped nanoclusters since two triplet C defects can form a quintuplet (Q) state as well. Here, we can observe first that the formation energy of the quintuplet states follows a similar tendency as triplet and singlet states; second, quintuplet states are less stable than singlet and triplet states.

To show the effect of carbon interactions on the electronic structure of C-doped H-SiNCs, the HOMO–LUMO gap is calculated for all 14 configurations, see Figure 3. For the antiferromagnetic states, the HOMO–LUMO gap depends on the site and the number of C atoms in the silicene nanocluster. Single C substitutions near the center have a larger effect on the band gap. For double C doping, the larger effects on the gap are shown near the edges due to correlation effects and structural relaxation. The results for the ferromagnetic states follow a similar trend to the antiferromagnetic state for single and double C substitutions.

Since dislocations and vacancies can arise as a consequence of imperfections during synthesis or stress imposed through thermal history,³⁶ we also calculated the formation energy for a dislocation and a monovacancy at position S_1 , see Figure 4. The formation energies for this dislocation are 5.082 and 5.021 eV, for the singlet and triplet state configurations, respectively. The band gap for the singlet and triplet state are 0.562 and 0.558 eV, respectively. For a monovacancy, the formation energy is 5.57 eV with a band gap of 0.405 eV. This shows the thermodynamically unstable nature of these defects.

Nanoscale length structures could differ considerably from their bulk counterparts in their physical and electronic properties; hence, caution must be taken when extrapolating results from finite to periodic structures. With this in mind, we have studied periodic boundary conditions of monolayers with supercell sizes of 2×2 , 3×3 , and 4×4 ; see the Supporting Information for more details. Formation energy and electronic structure properties were calculated using the PBE and B3LYP functionals. For the hybrid functional, B3LYP, we were able to obtain results for the 2×2 supercell due to the high computational cost of these calculations for bigger systems. For PBE, we obtained the formation energies -2.3609 , -2.4772 , and -2.5505 eV for the 2×2 , 3×3 , and 4×4 supercells,

Table 2. Formation Energies (in eV per impurity atom) of Double C Substitution at 13 Different Sites of H-SiNC for Singlet (S), Triplet (T), and Quintuplet (Q) States at the B3LYP Level of Calculation^a

site	2-C (S)	2-C (T)	2-C (Q)	1 + 1 C(S)	1 + 1 (T)	1 + 1 C (Q)
1	−5.710	−5.849	−4.992	−5.638	−5.793	−4.348
2	−5.752	−5.890	−5.097	−5.703	−5.840	−4.388
3	−6.177	−6.350	−5.525	−5.830	−5.957	−4.504
4	−5.651	−5.839	−5.057	−5.643	−5.794	−4.337
5	−5.655	−5.831	−5.001	−5.666	−5.803	−4.355
6	−5.634	−5.770	— ^b	−5.699	−5.870	−4.407
7	−5.865	−6.040	−5.190	−5.898	−6.032	−4.580
8	−5.997	−6.147	−5.418	−5.840	−5.979	−4.523
9	−5.823	−6.017	−5.191	−5.972	−6.120	−4.646
10	−5.805	−5.943	— ^b	−5.904	−6.053	−4.571
11	— ^b	−5.952	−5.155	−5.846	−5.986	−4.554
12	fixed	fixed	fixed	fixed	fixed	fixed
13	−6.592	−6.690	−5.828	−6.605	−6.725	−5.241
14	−6.242	−6.360	−5.550	−6.221	−6.492	−4.928

^aAll formation energies were calculated with respect to the singlet undoped ground state of H-SiNC(4,6). ^bStructures did not converge.

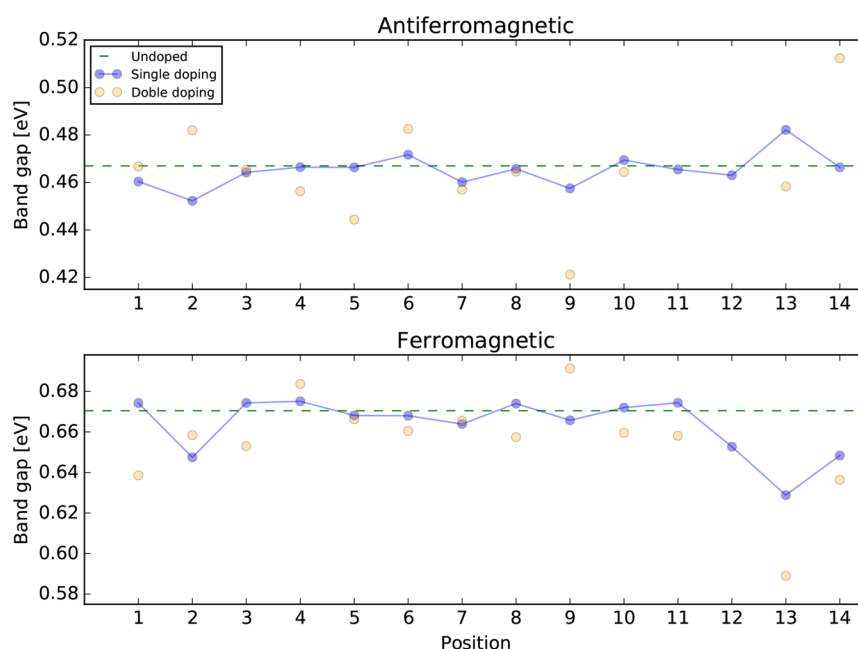


Figure 3. Calculated band gap of a rectangular silicene nanocluster, H-SiNC, for all 14 different positions. Antiferromagnetic and ferromagnetic states are illustrated for single and doubled C-doped structures. The dashed green lines in both graphs represent the band gap for the pristine cluster.

respectively; thus, these structures are thermodynamically favorable, in agreement with the nanoclusters calculations. The B3LYP calculations are in qualitative agreement and differ only by small amount with respect to the PBE functional.

Formation energies for double C substitution are reported in Table 3. Positions S_{12} and S_{13} are not considered here due to the size constraints of the supercells. B3LYP's results of double C substitution for a 2×2 supercell are shown in the Supporting Information. Formation energies shown in Table 3 follow the same trend as the nanoclusters. From the formation energies, we can see that the position S_8 is the most stable periodic structure as one may expect from a doping configuration that preserves most of the global symmetry of the layer. Also, for those structures in which the carbon atoms are located at the same sublattice, similar and larger band gaps are exhibited than those for which the doping occurs in opposite sublattices. This symmetry-breaking doping induces a

sublattice potential difference which in turn breaks the band degeneracy and opens the band gap.

Correlating Disorder and Interactions with Electronic Band Structures. As mentioned earlier, carbon substitutions introduce disorder and interactions that can affect the electronic structure. Here, we address the question of how the details of the band structure near the Dirac point are affected by disorder and interactions.

We select only the 2×2 supercell using the PBE functional. Figure 5a shows the band structure of different silicene structures alongside their respective density of states (DOS). In the following discussion, S_1 represents the only single-doped structure, while the rest of the mentioned positions stand for a double-doped structure with position S_1 fixed. Note that in the band structure calculations, different carbon positions generate different disorder and interaction strength which introduce a shift of the energy bands with respect to a reference case, i.e.,

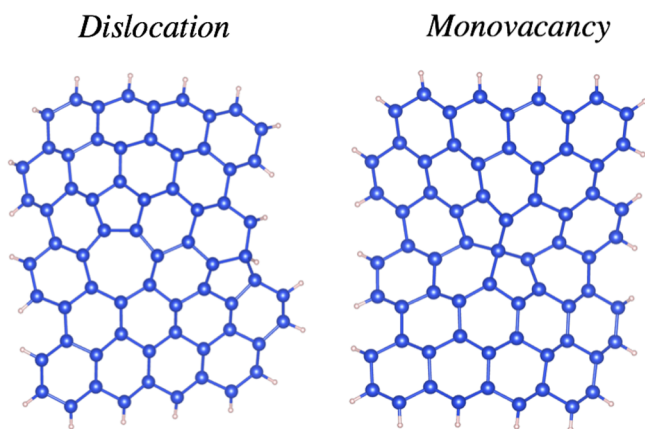


Figure 4. Geometry of a dislocation and a monovacancy in a silicene nanocluster. In both cases the structures shown are for singlet states configurations.

pristine silicene. For instance, when one silicene atom in the supercell is substituted by a carbon atom, a gap opens at the K point of 0.181 eV with a semiconductor behavior. Depending on the sublattice position, adding an additional carbon atom could break the symmetry of the system even more, resulting in a large band gap; this is the case for the S_1 – S_3 system (same sublattice) which shows an indirect gap of 1.006 eV and semiconductor behavior. On the other hand, the systems S_1 – S_4 and S_1 – S_8 act on different sublattices and show band gaps of 199 and 1 meV, respectively. Both systems present a direct gap; yet, the C4 gap is around the G point and C8 in the K direction. For the MV structure, we observe a metallic behavior, with a sizable direct band gap of 0.458 eV. Furthermore, we do not observe self-healing for any of the MV systems.

Understanding the Phase Transition. Using a toy model that captures the strength of electron interaction and the amount of disorder, we have calculated the local density of states (LDOS) around the Dirac point for the C-doped silicene structure. The LDOS in this model is

$$\rho_c(\omega) = \int \frac{d^2k}{(2\pi)^2} \delta(\omega - \epsilon_k - E_g(\omega, K_0, U)) \quad (2)$$

with

$$E_g(\omega, K_0, U) = \frac{K_0^2}{\omega - \tilde{\epsilon}_p + \frac{2U}{(\hbar v_F)^2} \frac{K_0^2}{(\omega - \tilde{\epsilon}_p)^2} \left(\omega - \frac{K_0^2}{\omega - \tilde{\epsilon}_p} \right)} \quad (3)$$

where $\tilde{\epsilon}_p = \epsilon_p - \frac{U}{2}$, $\epsilon_k = \hbar v_F |\mathbf{k}|$ is the energy dispersion at the K-point and $K_0^2 = \langle U_{\text{imp}}(\mathbf{r}_i) U_{\text{imp}}(\mathbf{r}_j) \rangle$ is the disorder correlator with $U_{\text{imp}}(\mathbf{r}_i)$ being the disorder potential strength. The energy of the p -electron is given by ϵ_p . The Hubbard U parameter describes the on-site interaction between two electrons with opposite spins on site i .

Using the proposed model we obtained the phase transition diagram for the Hubbard interaction U versus the strength of the disorder K_0 at zero temperature, see Figure 5b. Here, the two insulating phases are separated roughly by $U \propto 2K_0$. This means that the disorder affects the Mott transition by pushing it to larger interaction strength as also reported in refs 37 and 38. Figures 5c and 5d show the double-peak impurity resonances around the Fermi level for different disorder and interaction strengths. This type of double-peak structure has been experimentally observed in nitrogen-doped graphene and most likely originates from long-range interactions.³⁹ Indeed, the peak–peak separation goes down with increasing U . Eventually, for a large enough U , one of the resonance peaks moves past $\omega = 0$, where the Dirac point of the unperturbed system is located. In addition, Figure 5d reveals that there are more electronic states close to the Fermi level for higher disorders. This alternation between lower and higher densities of states brings out the fact that the two sublattices of silicene are affected differently by a substitutional atom (see the Supporting Information for consulting K_0 values). Hence, both the magnitude and the spatial range of the impurity potential are modified by interactions. Those results alongside DFT calculations help us to understand the driving factor for each system's transition.

In summary, we studied the effects of disorder on the electronic properties of silicene nanoclusters and monolayers caused by C doping. Total energies analysis indicates that C tends to be doped at the edges of finite silicene structures, which are ferromagnetic. Using field theory, we are able to describe the driving factor for different dope-induced transitions and to contrast its predictions with DFT results. Specifically, by looking at the band gap of the systems we are

Table 3. Formation Energies, E_f , and Band Gaps, E_g , of Double C Substitution for Spin-Polarized Systems at the PBE Level of Calculation^c

site	2 × 2		3 × 3		4 × 4	
	E_f (eV)	E_g (eV)	E_f (eV)	E_g (eV)	E_f (eV)	E_g (eV)
1	fixed	fixed	fixed	fixed	fixed	fixed
3	−5.4917	1.006 ^a	−5.0139	0.142	−5.0616	0.182
4	−4.0297	0.199 ^b	−4.1509	0.041	−4.2305	0.013
6	—	—	−4.8071	0.050	−4.9504	0.023
7	—	—	−5.6775	0.000	−5.4399	0.180
8	−6.2498	0.001 ^a	−5.6347	0.050	−5.5299	0.038
9	—	—	—	—	−4.9958	0.187
10	—	—	—	—	−5.3934	0.034
11	—	—	—	—	−5.4396	0.183
MV	2.9956	0.458 ^a	3.2189	0.003	3.2918	0.074

^aIndirect band gap. ^bDirect band gap. ^cHere, we use three different supercells. One C atom was fixed at position 1. The last row correspond to the monovacancy (MV) case.

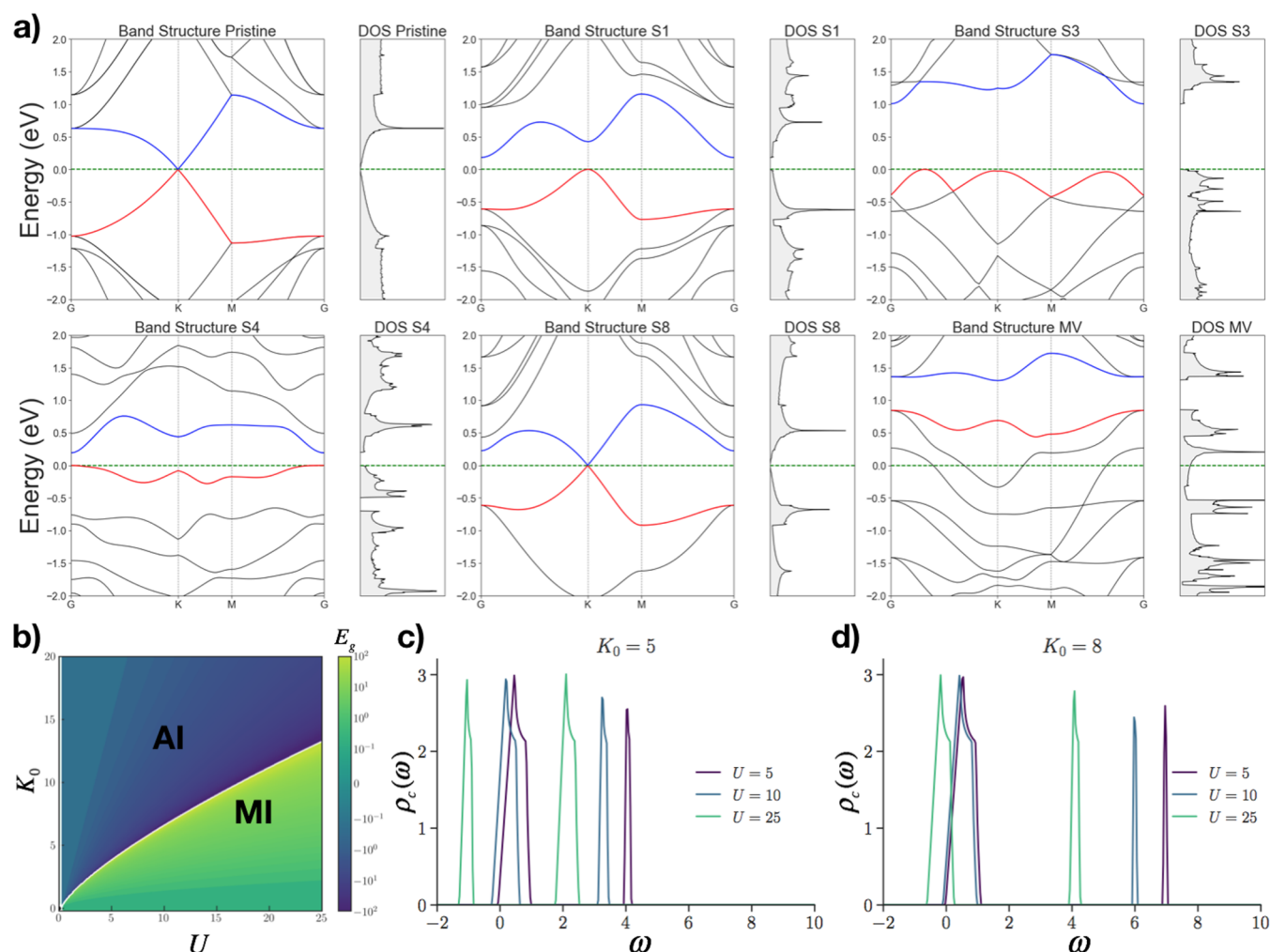


Figure 5. (a) The energy band structures and density of states (DOS) of periodic monolayers with different doping positions. The last figure correspond to the monovacancy (MV) case. The band structure was calculated along the path of the high symmetry points Γ – K – M – Γ . The blue and red lines represent the conduction and valence bands, respectively. The zero in the energy axis is set at the Fermi level as shown by the dashed green line. (b) Phase diagram in the K_0U plane for the Anderson–Hubbard model on the honeycomb lattice. AI and MI refer to the Anderson and Mott insulator, respectively. (c) LDOS of C-doped silicene at $K_0 = 5$ for varying the Hubbard interaction U . (d) Same as (c) for $K_0 = 8$.

able to distinguish between Anderson and Mott transitions. For a pristine silicene monolayer, the electronic dispersion is characterized by Dirac cones. Systems where the Hubbard interaction predominates break the degeneracy and crossing of the valence and conduction bands, hence opening a band gap; however, as the strength of the disorder increases, the gaps close, eventually recovering the presence of Dirac cones. This indicates that the Mott and Anderson insulators are continuously connected. The framework of our analysis not only applies to silicene but also other doped 2D materials.⁴⁰ Moreover, this combination of theoretical and computational results may be valuable in the design of silicene-based electronic devices in spintronics.^{32,33}

■ ASSOCIATED CONTENT

Supporting Information

The Supporting Information is available free of charge at <https://pubs.acs.org/doi/10.1021/acs.nanolett.0c01775>.

Formation energies for different C-doped silicene shapes, computational details for periodic silicene structures, and toy model for understanding the phase transition of the C-doped silicene systems (PDF)

■ AUTHOR INFORMATION

Corresponding Authors

Jose L. Mendoza-Cortes – Department of Chemical & Biomedical Engineering, FAMU-FSU Joint College of Engineering, Tallahassee, Florida 32310, United States; Department of Physics, Scientific Computing Department, Materials Science and Engineering, High Performance Material Institute, Condensed Matter Theory - National High Magnetic Field Laboratory, Florida State University, Tallahassee, Florida 32306, United States; orcid.org/0000-0001-5184-1406; Email: jmendoza@msu.edu

Troy Van Voorhis – Department of Chemistry, MIT, Cambridge, Massachusetts 02139, United States; orcid.org/0000-0001-7111-0176; Email: tvann@mit.edu

Authors

Ricardo Pablo-Pedro – Department of Chemistry and Department of Nuclear Science and Engineering, MIT, Cambridge, Massachusetts 02139, United States; orcid.org/0000-0003-4659-1996

Miguel Angel Magaña-Fuentes – Department of Chemical & Biomedical Engineering, FAMU-FSU Joint College of Engineering, Tallahassee, Florida 32310, United States

Marcelo Videia – School of Engineering and Sciences, Tecnológico de Monterrey, Monterrey 64849, Mexico

Jing Kong – Department of Electrical Engineering and Computer Science, MIT, Cambridge, Massachusetts 02139, United States;

orcid.org/0000-0003-0551-1208

Mingda Li – Department of Nuclear Science and Engineering, MIT, Cambridge, Massachusetts 02139, United States;

orcid.org/0000-0002-7055-6368

Complete contact information is available at:

<https://pubs.acs.org/10.1021/acs.nanolett.0c01775>

Notes

The authors declare no competing financial interest.

ACKNOWLEDGMENTS

R.P.-P., J.K., and T.V.V. acknowledge the King Abdullah University of Science and Technology for support under contract OSR-2015-CRG4-2634. R.P.-P. is thankful for the support from FEMSA and ITESM. J.L.M.-C. acknowledges start-up funds from Florida State University (FSU) and the Energy and Materials Initiative and facilities at the High Performance Material Institute (HPMI). Some of the computing for this project was performed on the HPC cluster at the Research Computing Center at the Florida State University (FSU). A portion of this work was performed at the National High Magnetic Field Laboratory, which is supported by National Science Foundation Cooperative Agreement no. DMR-1644779 and the State of Florida.

REFERENCES

- (1) Zhao, J.; Liu, H.; Yu, Z.; Quhe, R.; Zhou, S.; Wang, Y.; Liu, C. C.; Zhong, H.; Han, N.; Lu, J.; Yao, Y.; Wu, K. Rise of silicene: A competitive 2D material. *Prog. Mater. Sci.* **2016**, *83*, 24–151.
- (2) Ni, Z.; Liu, Q.; Tang, K.; Zheng, J.; Zhou, J.; Qin, R.; Gao, Z.; Yu, D.; Lu, J. Tunable Bandgap in Silicene and Germanene. *Nano Lett.* **2012**, *12*, 113–118.
- (3) Lalmi, B.; Oughaddou, H.; Enriquez, H.; Kara, A.; Vizzini, S.; Ealet, B.; Aufray, B. Epitaxial growth of a silicene sheet. *Appl. Phys. Lett.* **2010**, *97*, 223109.
- (4) Meng, L.; Wang, Y.; Zhang, L.; Du, S.; Wu, R.; Li, L.; Zhang, Y.; Li, G.; Zhou, H.; Hofer, W. A.; Gao, H.-J. Buckled Silicene Formation on Ir(111). *Nano Lett.* **2013**, *13*, 685–690.
- (5) Fleurence, A.; Friedlein, R.; Ozaki, T.; Kawai, H.; Wang, Y.; Yamada-Takamura, Y. Experimental Evidence for Epitaxial Silicene on Diboride Thin Films. *Phys. Rev. Lett.* **2012**, *108*, 245501.
- (6) Guzman-Verri, G. G.; Lew Yan Voon, L. C. Electronic structure of silicon-based nanostructures. *Phys. Rev. B: Condens. Matter Mater. Phys.* **2007**, *76*, 075131.
- (7) Cahangirov, S.; Topsakal, M.; Aktürk, E.; Şahin, H.; Ciraci, S. Two- and one-dimensional honeycomb structures of silicon and germanium. *Phys. Rev. Lett.* **2009**, *102*, 236804.
- (8) Kara, A.; Enriquez, H.; Seitonen, A. P.; Lew Yan Voon, L. C.; Vizzini, S.; Aufray, B.; Oughaddou, H. A review on silicene—New candidate for electronics. *Surf. Sci. Rep.* **2012**, *67*, 1–18.
- (9) Lin, Z.; Carvalho, B. R.; Kahn, E.; Lv, R.; Rao, R.; Terrones, H.; Pimenta, M. A.; Terrones, M. Defect engineering of two-dimensional transition metal dichalcogenides. *2D Mater.* **2016**, *3*, 022002.
- (10) Li, S.; Wu, Y.; Tu, Y.; Wang, Y.; Jiang, T.; Liu, W.; Zhao, Y. Defects in Silicene: Vacancy Clusters, Extended Line Defects, and Diatoms. *Sci. Rep.* **2015**, *5*, 7881.

(11) Rhodes, D.; Chae, S. H.; Ribeiro-Palau, R.; Hone, J. Disorder in van der Waals heterostructures of 2D materials. *Nat. Mater.* **2019**, *18*, 541.

(12) Chen, J.-H.; Jang, C.; Adam, S.; Fuhrer, M.; Williams, E.; Ishigami, M. Charged-impurity scattering in graphene. *Nat. Phys.* **2008**, *4*, 377.

(13) Sachs, B.; Britnell, L.; Wehling, T.; Eckmann, A.; Jalil, R.; Belle, B.; Lichtenstein, A.; Katsnelson, M.; Novoselov, K. Doping mechanisms in graphene-MoS₂ hybrids. *Appl. Phys. Lett.* **2013**, *103*, 251607.

(14) Rosenbaum, T. F.; Milligan, R. F.; Paalanen, M. A.; Thomas, G. A.; Bhatt, R. N.; Lin, W. Metal-insulator transition in a doped semiconductor. *Phys. Rev. B: Condens. Matter Mater. Phys.* **1983**, *27*, 7509–7523.

(15) MOTT, N. F. Metal-Insulator Transition. *Rev. Mod. Phys.* **1968**, *40*, 677–683.

(16) Anisimova, S.; Kravchenko, S. V.; Punnoose, A.; Finkel'stein, A. M.; Klapwijk, T. M. Flow diagram of the metal–insulator transition in two dimensions. *Nat. Phys.* **2007**, *3*, 707.

(17) Lilly, M. P.; Reno, J. L.; Simmons, J. A.; Spielman, I. B.; Eisenstein, J. P.; Pfeiffer, L. N.; West, K. W.; Hwang, E. H.; Das Sarma, S. Resistivity of dilute 2D electrons in an undoped GaAs heterostructure. *Phys. Rev. Lett.* **2003**, *90*, 056806.

(18) Limelette, P.; Wzietek, P.; Florens, S.; Georges, A.; Costi, T.; Pasquier, C.; Jérôme, D.; Mézière, C.; Batail, P. Mott Transition and Transport Crossovers in the Organic Compound κ -(BEDT-TTF)₂ Cu[N(CN)₂]Cl. *Phys. Rev. Lett.* **2003**, *91*, 016401.

(19) Zwerger, W. Mott–Hubbard transition of cold atoms in optical lattices. *J. Opt. B: Quantum Semiclassical Opt.* **2003**, *5*, S9.

(20) Evers, F.; Mirlin, A. D. Anderson transitions. *Rev. Mod. Phys.* **2008**, *80*, 1355–1417.

(21) Shi, Z.; Zhang, Z.; Kutana, A.; Yakobson, B. I. Predicting Two Dimensional Silicon Carbide Monolayers. *ACS Nano* **2015**, *9*, 9802.

(22) Vahabzadeh, N.; Alaei, H. R. Ab-initio study of electronic properties of Si(C) honeycomb structures. *Chin. J. Phys.* **2019**, *57*, 479–489.

(23) Grimme, S.; Antony, J.; Ehrlich, S.; Krieg, H. A consistent and accurate ab initio parametrization of density functional dispersion correction (DFT-D) for the 94 elements H–Pu. *J. Chem. Phys.* **2010**, *132*, 154104.

(24) Shao, Y.; Gan, Z.; Epifanovsky, E.; Gilbert, A. T.; Wormit, M.; Kussmann, J.; Lange, A. W.; Behn, A.; Deng, J.; Feng, X.; et al. Advances in molecular quantum chemistry contained in the Q-Chem 4 program package. *Mol. Phys.* **2015**, *113*, 184–215.

(25) Kresse, G.; Hafner, J. Ab initio molecular dynamics for liquid metals. *Phys. Rev. B: Condens. Matter Mater. Phys.* **1993**, *47*, 558–561.

(26) Kresse, G.; Hafner, J. Ab initio molecular-dynamics simulation of the liquid-metal–amorphous-semiconductor transition in germanium. *Phys. Rev. B: Condens. Matter Mater. Phys.* **1994**, *49*, 14251–14269.

(27) Kresse, G.; Furthmüller, J. Efficiency of ab-initio total energy calculations for metals and semiconductors using a plane-wave basis set. *Comput. Mater. Sci.* **1996**, *6*, 15–50.

(28) Kresse, G.; Furthmüller, J. Efficient iterative schemes for ab initio total-energy calculations using a plane-wave basis set. *Phys. Rev. B: Condens. Matter Mater. Phys.* **1996**, *54*, 11169–11186.

(29) Monkhorst, H. J.; Pack, J. D. Special points for Brillouin-zone integrations. *Phys. Rev. B* **1976**, *13*, 5188.

(30) Pablo-Pedro, R.; Lopez-Rios, H.; Fomine, S.; Dresselhaus, M. S. Detection of Multiconfigurational States of Hydrogen-Passivated Silicene Nanoclusters. *J. Phys. Chem. Lett.* **2017**, *8*, 615–620.

(31) Ma, L.; Zhang, J.-M.; Xu, K.-W.; Ji, V. Structural and electronic properties of substitutionally doped armchair silicene nanoribbons. *Phys. B* **2013**, *425*, 66–71.

(32) Han, W.; Kawakami, R. K.; Gmitra, M.; Fabian, J. Graphene spintronics. *Nat. Nanotechnol.* **2014**, *9*, 794.

(33) Pesin, D.; MacDonald, A. H. Spintronics and pseudospintronics in graphene and topological insulators. *Nat. Mater.* **2012**, *11*, 409.

(34) Jansen, R. Silicon spintronics. *Nat. Mater.* **2012**, *11*, 400.

(35) Pablo-Pedro, R.; Lopez-Rios, H.; Mendoza-Cortes, J.-L.; Kong, J.; Fomine, S.; Van Voorhis, T.; Dresselhaus, M. S. Exploring low internal reorganization energies for silicene nanoclusters. *Phys. Rev. Appl.* **2018**, *9*, 054012.

(36) Li, S.; Wu, Y.; Tu, Y.; Wang, Y.; Jiang, T.; Liu, W.; Zhao, Y. Defects in silicene: vacancy clusters, extended line defects, and diadatoms. *Sci. Rep.* **2015**, *5*, 7881.

(37) Byczuk, K.; Hofstetter, W.; Vollhardt, D. Mott-Hubbard Transition versus Anderson Localization in Correlated Electron Systems with Disorder. *Phys. Rev. Lett.* **2005**, *94*, 056404.

(38) Haase, P.; Yang, S.-X.; Pruschke, T.; Moreno, J.; Jarrell, M. Dual-fermion approach to the Anderson-Hubbard model. *Phys. Rev. B: Condens. Matter Mater. Phys.* **2017**, *95*, 045130.

(39) Joucken, F.; Tison, Y.; Lagoute, J.; Dumont, J.; Cabosart, D.; Zheng, B.; Repain, V.; Chacon, C.; Girard, Y.; Botello-Méndez, A. R.; Rousset, S.; Sporken, R.; Charlier, J.-C.; Henrard, L. Localized state and charge transfer in nitrogen-doped graphene. *Phys. Rev. B: Condens. Matter Mater. Phys.* **2012**, *85*, 161408.

(40) Usachov, D.; Vilkov, O.; Gruneis, A.; Haberer, D.; Fedorov, A.; Adamchuk, V.; Preobrajenski, A.; Dudin, P.; Barinov, A.; Oehzelt, M.; et al. Nitrogen-doped graphene: efficient growth, structure, and electronic properties. *Nano Lett.* **2011**, *11*, 5401–5407.